

PAPER • OPEN ACCESS

Influence of cell shape, inhomogeneities and diffusion barriers in cell polarization models

To cite this article: Wolfgang Giese *et al* 2015 *Phys. Biol.* **12** 066014

View the [article online](#) for updates and enhancements.

You may also like

- [A biomechanical model for the transendothelial migration of cancer cells](#)
S M Amin Arefi, Daria Tsvirkun, Claude Verdier *et al.*
- [A Rho-GTPase based model explains group advantage in collective chemotaxis of neural crest cells](#)
Brian Merchant and James J Feng
- [Calcium oscillations in blood platelets and their possible role in 'interpreting' extracellular information by cells](#)
S S Shakhidzhanov, F A Balabin, S I Obydenny *et al.*



 EDINBURGH INSTRUMENTS

WORLD LEADING MOLECULAR SPECTROSCOPY SOLUTIONS

edinst.com

Physical Biology



PAPER

Influence of cell shape, inhomogeneities and diffusion barriers in cell polarization models

OPEN ACCESS

RECEIVED

13 April 2015

REVISED

5 August 2015

ACCEPTED FOR PUBLICATION

10 August 2015

PUBLISHED

23 November 2015

Content from this work may be used under the terms of the [Creative Commons Attribution 3.0 licence](#).

Any further distribution of this work must maintain attribution to the author(s) and the title of the work, journal citation and DOI.



Wolfgang Giese^{1,5}, Martin Eigel^{2,5}, Sebastian Westerheide³, Christian Engwer^{3,4} and Edda Klipp¹

¹ Theoretical Biophysics, Humboldt-Universität zu Berlin, Berlin, Germany

² Weierstrass Institute, Berlin, Germany

³ Institute for Computational and Applied Mathematics, University of Münster, Münster, Germany

⁴ Cells in Motion (CiM) Cluster of Excellence EXC 1003, University of Münster, Münster, Germany

⁵ These authors contributed equally to this work

E-mail: edda.klipp@rz.hu-berlin.de

Keywords: polarization models, spatial simulation, spatial inhomogeneities, Cdc42, yeast

Supplementary material for this article is available [online](#)

Abstract

In silico experiments bear the potential for further understanding of biological transport processes by allowing a systematic modification of any spatial property and providing immediate simulation results. Cell polarization and spatial reorganization of membrane proteins are fundamental for cell division, chemotaxis and morphogenesis. We chose the yeast *Saccharomyces cerevisiae* as an exemplary model system which entails the shuttling of small Rho GTPases such as Cdc42 and Rho, between an active membrane-bound form and an inactive cytosolic form. We used partial differential equations to describe the membrane-cytosol shuttling of proteins. In this study, a consistent extension of a class of 1D reaction-diffusion systems into higher space dimensions is suggested. The membrane is modeled as a thin layer to allow for lateral diffusion and the cytosol is modeled as an enclosed volume. Two well-known polarization mechanisms were considered. One shows the classical Turing-instability patterns, the other exhibits wave-pinning dynamics. For both models, we investigated how cell shape and diffusion barriers like septin structures or bud scars influence the formation of signaling molecule clusters and subsequent polarization. An extensive set of *in silico* experiments with different modeling hypotheses illustrated the dependence of cell polarization models on local membrane curvature, cell size and inhomogeneities on the membrane and in the cytosol. In particular, the results of our computer simulations suggested that for both mechanisms, local diffusion barriers on the membrane facilitate Rho GTPase aggregation, while diffusion barriers in the cytosol and cell protrusions limit spontaneous molecule aggregations of active Rho GTPase locally.

Introduction

Fundamental processes of living cells such as cell division, chemotaxis and morphogenesis depend on prior polarization and breaking of spatial symmetry. Spatial reorganization of membrane-bound and cytosolic proteins is required to establish an axis of polarity with a distinct direction (i.e. 'front and back') to guide directed processes. In these processes, cells have to adapt and react according to multiple and often conflicting cues of the environment.

Rapid technical development makes it possible to observe these processes in great detail *in vivo*. Advances in imaging techniques such as total internal reflection

fluorescence (TIRF) and confocal and electron microscopy [1–4] provide quantitative data for spatial cellular structures such as diffusion barriers on the membrane, organelles and membranes in the cytosol. To enhance the experiment-theory feedback loop, new computational tools have to be developed, to reconstruct the observed cell shapes, spatial inhomogeneities and structures at different levels of biological detail and mathematical complexity [5]. Quantitative modeling of intracellular asymmetries and inhomogeneities is essential for testing hypotheses, for obtaining an intuition of the process as well as for motivating new experimental studies.

The theoretical treatment of cell polarization has been devoted to biological model organisms such as

yeast, fish keratocytes, *Dictyostelium discoideum* or neutrophils. Much recent work is concerned with reaction-diffusion (RD) models which are often described by partial differential equations (PDEs) in time and space as in [6–15]. Such models may vary greatly in complexity. Some of them are based on biochemical networks with many components [11, 12, 14, 15] gathered from signaling pathway databases. Other models focus on only a few components to accurately describe cell behavior. Detailed reviews of models for yeast cell polarity can be found in [5, 16].

The above sets of models pursue different goals. Since biochemical complexity can become overwhelmingly large, the experimental validation of generated models of high complexity is basically impossible [17, 18] and an accurate spatial simulation becomes prohibitively costly. The alternative is to reduce signaling pathways to very few interacting constituents which still exhibit the specific behavior one is interested in. This simplified system can then be simulated subject to a spatio-temporal mathematical model which also includes (some) geometrical properties encountered in living cells. Ideally, *in vivo* or *in vitro* phenomena can be reconstructed, rates and concentrations can be compared and matched.

Since Meyers *et al* [19] showed the potential influence of cell shape and size on signaling, a growing number of models take into account the interaction of biochemical signaling and cell geometry [20, 21]. More recently, some studies investigated the interplay of cell motility and signaling [22–25] in a 2D or 3D environment. There have been a lot of advances in computational frameworks for complex simulations in 2D and 3D. In particular, we want to mention VCell [26] dedicated to cell biology and DUNE [27] as a general purpose framework; the latter was used in this work. An interesting review on multiphysics models at different levels of complexity can be found in [28]. Examples where microscopic imaging and spatial modeling of cell shape and signaling are connected are shown in [29–31]. However, there are still a lot of aspects that need physical and computational analysis, among them inhomogeneous diffusion caused by organelles and other cellular inclusions.

Spatial structures such as organelles, diffusion barriers on the membrane and cell shape are expected to have a considerable influence on cell polarization. In [19, 32, 33], it was shown that high intracellular cytosolic gradients can be generated. Even though diffusion in the cytosol might be fast in theory, it can differ a lot from the effective diffusion rate due to obstacles such as large organelles, membrane structures or a crowded environment [34]. Therefore, it is important to incorporate intracellular gradients and diffusion as a spatial process in the cytosol [35–37]. Furthermore, membrane inhomogeneities are likely to have an effect on signaling as well [38].

To include the mentioned spatial properties in our modeling, we present an advanced computational

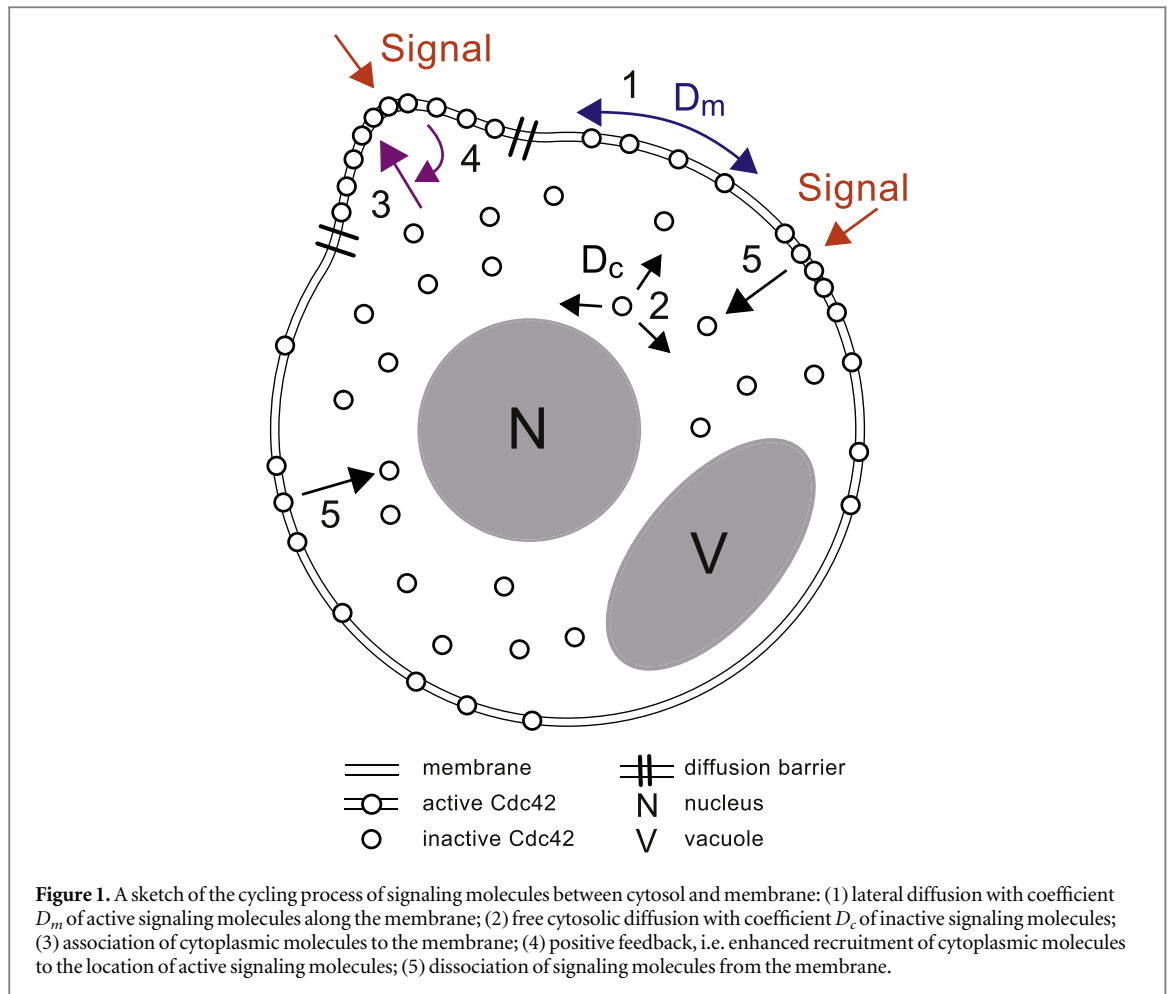
approach to simulate RD models which take into account important aspects of spatial complexity. In our modeling approach spatial inhomogeneities such as organelles or bud scars are represented by an inhomogeneous diffusion coefficient or as inner boundaries in the computational domain. The RD model equations connect membrane and cytosol by coupling terms which represent reaction kinetics on the membrane and depend on the concentration of membrane-bound and cytosolic species. In comparison to the cytosol, the cell membrane is modeled as a thin layer to allow for diffusion in lateral direction only [39]. Furthermore, we are not restricted to a circular or elliptical geometry but can choose any shape.

Our computational approach relates to recent advances in surface finite element methods (SFEM) [29, 40] which also take into account surface curvature of the membrane. With these methods, the RD model equations can be solved with high accuracy and great flexibility regarding the spatial geometry.

Modeling yeast cell polarity

A prominent example for cell polarization is the yeast budding process. The location of bud formation is specified by cortical landmark proteins Rsr1/Bud1, which are inherited from the previous cell division. One key molecule during this process is the Rho GTPase Cdc42. In the absence of Cdc42, cells fail to polarize, remain circular and are, therefore, unable to form a bud [41]. As known from all Rho GTPases, Cdc42 cycles between an active GTP-bound and an inactive GDP-bound state. A prenyl group anchors Cdc42 into the membrane where it can diffuse slowly. Cdc42 can be pulled out of the membrane by Rdi1, its guanosine nucleotide dissociation inhibitor (GDI). Active Cdc42-GTP levels can be upregulated by guanine nucleotide exchange factors (GEFs) or reduced by GTPase-activating proteins (GAPs). In the course of these interactions, a unique polarization cap of active Cdc42 is generated on the cell membrane which initiates the emerging bud on the site of the polarization cap [14]. A sketch of this process is shown in figure 1.

Interestingly, the normal bud site selection machinery, in which the bud scar from the previous cell division determines the direction of budding, could be perturbed systematically in a number of experiments. First, it could be shown that overexpression of the active form of Cdc42 leads to phenotypes that polarize randomly at multiple spots and also grow more than one bud [42]. Second, deleting the landmark protein Rsr1 still yields a polarization cap which randomly explores the cell periphery. Additional treatment with latrunculin A, an actin-depolymerizing drug, causes cells to spontaneously polarize and establish a random but stable axis of polarity [7].



This indicates that polarization is possible without actin-driven rearrangements of Cdc42.

In *S. cerevisiae*, an alternative pathway that leads to Cdc42 activation is induced by the heterotrimeric G protein signaling during the mating process [43]. Here, shallow pheromone gradients cause the yeast cell to grow a projection (called shmoo) in the direction of a mating partner. In this case, Far1p associates with the $G\beta\gamma$ subunits which leads to the accumulation of Cdc42p at the site of receptor stimulation. Even when stimulated with conflicting or noisy pheromone signals, cells are still able to form a single shmoo in an arbitrary direction [30].

The cell-type specific details of the spatial molecule cycling can be very complex. For instance, signaling molecules can associate to the plasma membrane through membrane anchoring, binding to phospholipid headgroups or docking with transmembrane receptors. To be able to find generic properties of cell polarization, we aim to investigate abstracted mechanisms that represent generic features of eukaryotic cell polarization. A detailed review of polarization models for various cell types can be found in [16]. We are going to investigate basic mechanisms of Turing-type [8, 11] and wave-pinning type [7, 10], which have both been suggested for yeast.

As the first mechanism of Turing-type, we tested the model from Goryachev and Pokhilko [11] and refer to it as GOR model. This model was derived in a bottom-up approach that takes all actin-independent components of the yeast polarization machinery into account. Analysis and reduction of the model led to a Turing-type mechanism for yeast polarization with just two components. The system starts in a homogeneous steady state which is unstable with respect to minute spatial perturbations and runs into a spatially inhomogeneous polarized state. Such perturbations may be small localized cues or spontaneous association of active molecules to the membrane.

As the second mechanism, we tested the wave-pinning (WP) model which was first suggested in Mori et al [10]. This model is an abstracted caricature of the shuttling of Rho GTPases. It has been used to characterize the polarization behavior of various cell types from neutrophils to *Dictyostelium discoideum* and also yeast. Experimental evidence for traveling waves of active Cdc42 were observed for instance in Ozbudak et al [7]. In the WP model, the corresponding homogeneous system has two stable and one unstable transient steady state. The steady state at lower concentration of active membrane-bound molecules corresponds to an unexcited state, while the steady state at higher surface concentration corresponds to

an excited state. Stimulation of the system causes traveling waves on the cell surface that are pinned into a polar stable state due to global mass conservation. However, the stimulation needs to exceed a certain threshold to drive the system from a homogeneous unpolarized state into a polar state.

In this work, we examined and illustrated the importance of spatial properties such as cell shape, cell size, inhomogeneities on the membrane and the location of (large) organelles in the cytosol for the two models described above. There is still a debate about which kind of model is most appropriate to capture the main features of yeast polarization and which is best suited to develop an intuition of the polarization process in various situations [5]. Both models, WP and GOR, were tested in setups relevant to the polarization behavior of mating and budding yeast *Saccharomyces cerevisiae*.

Modeling approach for a class of mass conservative reaction-diffusion mechanisms

A traditional way to understand basic mechanisms of cell polarity is the investigation of RD models where the geometry of the cell is reduced to one space dimension. With models of this kind, basic features of the reaction-diffusion dynamics can be captured. The cell is represented by an interval $[0, L]$ which can be either interpreted as the circumference [44] of the cell or as a cell diameter transect [16].

In the first case, the ends of the interval are glued together and periodic boundary conditions are employed. In the second case, the boundary of the interval represents front and back of the cell. In the following model, the concentration of active Rho GTPase (GTP, membrane-bound) is denoted by $u(x, t)$ and the concentration of inactive Rho GTPase (GDP, cytosolic) is denoted by $v(x, t)$. Using the interpretation as a cell diameter transect, the set of RD equations to describe the spatial dynamics reads

$$\frac{\partial u}{\partial t} = D_m \frac{\partial^2 u}{\partial x^2} + f(u, v), \quad x \in [0, L], t \in [0, T], \quad (1)$$

$$\frac{\partial v}{\partial t} = D_c \frac{\partial^2 v}{\partial x^2} - f(u, v), \quad (2)$$

with some initial values $u(\cdot, 0)$ and $v(\cdot, 0)$ in $[0, L]$ and no-flux boundary conditions

$$\frac{\partial u}{\partial x}(0, t) = \frac{\partial u}{\partial x}(L, t) = \frac{\partial v}{\partial x}(0, t) = \frac{\partial v}{\partial x}(L, t) = 0. \quad (3)$$

A comparison and analysis of different reduced models can be found in [16, 45].

A drawback of these 1D models is that they neglect potentially important details of the cell geometry, whereas models in 2D or 3D can also account for the

spatial structure of a cell. We thus investigate higher dimensional models and focus on the 2D case in this article.

In the geometric representation of the cell, we incorporate the cell membrane, the cytosol and inner membranes that enclose organelles like the vacuole or the nucleus. We assume free diffusion of molecules in the cytosol which is limited by the outer cell membrane, M^{cell} , and the inner membranes, M^{org} , of the organelles. The cytosolic volume is denoted by V^{cyt} and its boundary surface is $\partial V^{\text{cyt}} = M^{\text{cell}} \cup M^{\text{org}}$ (see figure S1).

Here, ∂D denotes the boundary of some domain D . The active membrane-bound form of the signaling molecule is represented by its concentration $u(\vec{x}, t)$ and the inactive cytosolic form is represented by its concentration $v(\vec{x}, t)$. These are both functions of space $\vec{x} \in M^{\text{cell}} \subset \mathbb{R}^2$ or $\vec{x} \in V^{\text{cyt}} \subset \mathbb{R}^2$ and time $t \in [0, T]$, where $T > 0$ is the end time. In brief, in the two-dimensional case, the plasma membrane is represented as a one-dimensional curve enveloping the two-dimensional cytosolic domain.

With this geometric representation of the cell, the shuttling between membrane-bound and cytosolic signaling molecules is naturally described by a flux at the membrane-cytosolic interface which follows specific reaction kinetics depending on concentrations u and v . The model is formulated as the system of partial differential equations

$$\frac{\partial u}{\partial t} = \nabla_{\Gamma} \cdot (D_m \nabla_{\Gamma} u) + f(u, v) \text{ on } M^{\text{cell}} \times [0, T], \quad (4)$$

$$\frac{\partial v}{\partial t} = \nabla \cdot (D_c \nabla v) \text{ in } V^{\text{cyt}} \times [0, T]. \quad (5)$$

The boundary conditions for the cytosolic equation (5) read

$$-D_c \nabla v \cdot \vec{n} = f(u, v) \text{ on } M^{\text{cell}} \times [0, T], \quad (6)$$

$$-D_c \nabla v \cdot \vec{n} = 0 \text{ on } M^{\text{org}} \times [0, T]. \quad (7)$$

Here, \vec{n} denotes the vector field of outer unit normals on M^{cell} and M^{org} , respectively. Moreover, the initial concentrations at time $t=0$ are given by

$$u(\vec{x}, 0) = u_0(\vec{x}) \quad \text{and} \quad v(\vec{x}, 0) = v_0(\vec{x}). \quad (8)$$

These equations comprise three types of processes which occur simultaneously: (a) Diffusion of $u(\vec{x}, t)$ on the curved membrane where the diffusion coefficient $D_m(\vec{x})$ is a function in space in order to allow for position dependent diffusivity and ∇_{Γ} denotes the surface gradient operator in \vec{x} which accounts for curvature of Γ , see [40]. (b) Diffusion of $v(\vec{x}, t)$ in the cytosol with diffusion coefficient $D_c(\vec{x})$ where ∇ denotes the usual gradient operator in \vec{x} with respect to standard Cartesian coordinates in Euclidean space. (c) The reaction processes on the membrane described by a flux at the membrane-cytosolic interface with density $J = f(u, v)$ are modeled as a source term for the membrane-bound complex in equation (4) and as

Table 1. Overview of variables and constants. Note that $1 \mu M = 10^{-21} \text{ mol}/\mu\text{m}^3 \approx 602 \text{ molec}/\mu\text{m}^3$ are the units for the cytosolic species v in the bulk and $1 \mu\text{m} \mu M = 10^{-21} \text{ mol}/\mu\text{m}^2 \approx 602 \text{ molec}/\mu\text{m}^2$ are the units for the membrane-bound species u .

Model	Parameter/entity	Value	Unit	Description
GOR & WP	u	—	$\mu\text{m} \mu M$	concentration of the membrane-bound species
	v	—	μM	concentration of the cytosolic species
	$f(u, v)$	—	$\mu\text{m} \mu M/s$	density of flux at the membrane-cytosolic interface
	D_m	—	$\mu\text{m}^2/s$	diffusion coefficient for the membrane-bound species
	D_c	—	$\mu\text{m}^2/s$	diffusion coefficient for the cytosolic species
GOR	α	3.3	$\mu\text{m}^{-1} \mu M^{-2} s^{-1}$	cooperative positive feedback
	β	0.67	$\mu M^{-1} s^{-1}$	noncooperative binding to membrane
	γ	0.017	$1/s$	rate of basal dissociation from membrane
	E_c	0.1	-	membrane-bound Cdc24-Bem1 complex
WP	k_0	0.067	$\mu\text{m}/s$	rate of basal activation
	δ	1.0	$1/s$	rate of basal dissociation
	γ	1.0	$\mu\text{m}/s$	maximal rate of auto-activation of u
	K	0.1	$\mu\text{m} \mu M$	concentration of u resulting in half-maximal rate of auto-activation

a Robin-like boundary condition for the cytosolic concentration $v(\vec{x}, t)$ in equation (6). The cytosolic species v only interacts with the membrane-bound species u on the cell membrane M^{cell} . Hence, there is no extra reaction term in the volume equation (5). Note that the typical units of the membrane-bound species u are molecules per area and for the cytosolic species v molecules per volume. Thus, the flux $f(u, v)$ naturally obtains the unit molecules per area and time.

For $f(u, v) > 0$ we obtain a flux from the cytosol onto the membrane whereas for $f(u, v) < 0$ the active form u dissociates into the cytosol. We use the term

$$f(u, v) := f^{\text{cyc}}(u, v) + k_S v, \quad (9)$$

where $f^{\text{cyc}}(u, v)$ represents the reaction kinetics of the model's basic reaction mechanism. The function k_S is positive and depends on space and time, i.e. $k_S(\vec{x}, t) \in \mathbb{R}^+$. It accounts for signals that excite the system and cause a flux from cytosol to membrane. The signal settings in this paper vary from conflicting localized stimuli, graded signals to external noise (see Methods section).

Since the source term in equation (4) and boundary condition (6) balance each other, this system of equations is mass conservative. This means that the total mass of the considered signaling molecule is constant in time, i.e.

$$\underbrace{\int_{M^{\text{cell}}} u \, dA}_{\text{mass on the cell membrane}} + \underbrace{\int_{V^{\text{cyl}}} v \, dV}_{\text{mass in the cytosol}} = M \quad (10)$$

for each $t \in [0, T]$, where $M \in \mathbb{R}$. A derivation can be found in supplementary material S1. Note that in the two-dimensional case, which is considered in this work, the surface integral is an integral along the one-dimensional curve enveloping the cell and the volume integral is an integral over a two-dimensional domain, which represents a slice of the cell. Therefore, the unit for M becomes molecules per height. To obtain actual

molecule numbers in the cell slice, M needs to be integrated along the height of the cell slice.

In the general framework for cell polarization models, the reaction kinetics $f^{\text{cyc}}(u, v)$ incorporates a self-amplifying feedback on the active membrane-bound species u . The location where most active signaling molecules are accumulated also recruits the most inactive signaling molecules from the cytosol. This has to be understood as a competition between different polarization sites since the cytosolic pool of inactive molecules is limited. There are several different model realizations for $f^{\text{cyc}}(u, v)$ with different properties [8, 10, 11].

We employ the kinetics of the GOR [11] and WP [10] models in the remainder of this study. The GOR model [11, 14, 16] represents a Turing-type mechanism and was derived as a simplification of a detailed biochemical signaling pathway involved in the yeast budding process. It employs the reaction kinetics

$$\begin{aligned} f^{\text{cyc}}(u, v) &= f^{\text{GOR}}(u, v) \\ &:= \alpha E_c u^2 v + \beta E_c u v - \gamma u. \end{aligned} \quad (11)$$

The terms $\alpha E_c u^2 v$ and $\beta E_c u v$ account for the positive feedback loop of Rho GTPase activation mediated by the corresponding GEFs. The first nonlinear term additionally assumes a cooperative effect of the active form of the Rho GTPases onto its own production. The dissociation of the membrane-bound Rho GTPase mediated by its GAPs and GDIs is described by the degradation term γu . The factors α , β and γ are constants. E_c accounts for the Bem1-Cdc24 complex occurring in yeast and it is assumed constant for simplicity, see also [16]. For a cell of $5 \mu\text{m}$ diameter, Cdc42 molecule numbers in the order of 10^5 are assumed in [11]. However, recent measurements [9, 15, 46] have reported lower Cdc42 molecule numbers in the order of 10^3 to 10^4 . Therefore, we rescaled the parameter values from [11] (see table 1). The function $f^{\text{GOR}}(u, v)$ is plotted in figure S2 (see

Table 2. Sets of diffusion coefficients.

model	parameter	value		description
GOR	D_m^{GOR}	0.0025	$\mu\text{m}^2/\text{s}$	diffusion coefficients used in [11]
	D_c^{GOR}	1.0 – – 10.0	$\mu\text{m}^2/\text{s}$	
WP	D_m^{WP}	0.1	$\mu\text{m}^2/\text{s}$	diffusion coefficients used in [10]
	D_c^{WP}	10.0	$\mu\text{m}^2/\text{s}$	
GOR & WP	D_m^{cons}	0.015	$\mu\text{m}^2/\text{s}$	consensus diffusion coefficients used in this work (geometric mean of extreme values found in the references)
	D_c^{cons}	3.0	$\mu\text{m}^2/\text{s}$	

supplementary material S1) for fixed values of v . We chose $v_0 \equiv 0.2 \mu\text{M}$ and $u_0 \equiv 0.054 \mu\text{m} \mu\text{M}$ as initial conditions for the GOR model throughout this paper. This corresponds to the non-zero homogeneous steady state of the system.

The WP model was thoroughly investigated in [10, 16, 47, 48]. Its reaction kinetics reads

$$f^{\text{cyc}}(u, v) = f^{\text{WP}}(u, v) \\ := v \left(k_0 + \frac{\gamma u^2}{K^2 + u^2} \right) - \delta u. \quad (12)$$

The nonlinear Hill-Term $\gamma u^2 / (K^2 + u^2)$ accounts for cooperative effects of membrane-bound Rho GTPase activation which is mediated by its GEFs. Here, the constants γ and K represent the maximal activation rate and the concentration of half occupation. The basal GEF activation rate is expressed by k_0 . The inactivation and dissociation of the membrane-bound Rho GTPase mediated by its GAPs and GDIs is described by the degradation term δu . As with the GOR model, the reaction kinetics is plotted in figure S2 for fixed values of v and the kinetic parameters are shown in table 1. In the original work of Mori *et al* [10], both u and v were treated as effective concentrations with the same units along a 1D cell transect. Here, u represents a surface concentration on the membrane and v a bulk concentration in the cytosol. Therefore, we adapted the units of the parameters k_0 , γ and K accordingly. Furthermore, we rescaled the parameter K to be in a comparable regime of concentrations as with the GOR model. In all experiments we used $v_0 \equiv 0.2 \mu\text{M}$ and $u_0 \equiv 0.026 \mu\text{m} \mu\text{M}$ as initial conditions for the WP model, which corresponds to the stable unexcited homogeneous steady state of the system. It should be noted that for fixed cytosolic concentration $v_0 \equiv 0.2 \mu\text{M}$, the kinetic term $f(v_0, u)$ has three roots $u^- < u^T < u^+$. The first corresponds to a stable unexcited, the second to an unstable transient and the third to a stable and excited state of the system.

In the original works from Goryachev and Pokhilko [11], and Mori *et al* [10], different values for the diffusion coefficients were used even though both refer to measured values in the model organism yeast. Each set D_m^{GOR} and D_m^{WP} of considered diffusion coefficients can be compared using table 2. The membrane diffusion coefficients vary about a factor of 40. These discrepancies have been inherited in recent literature.

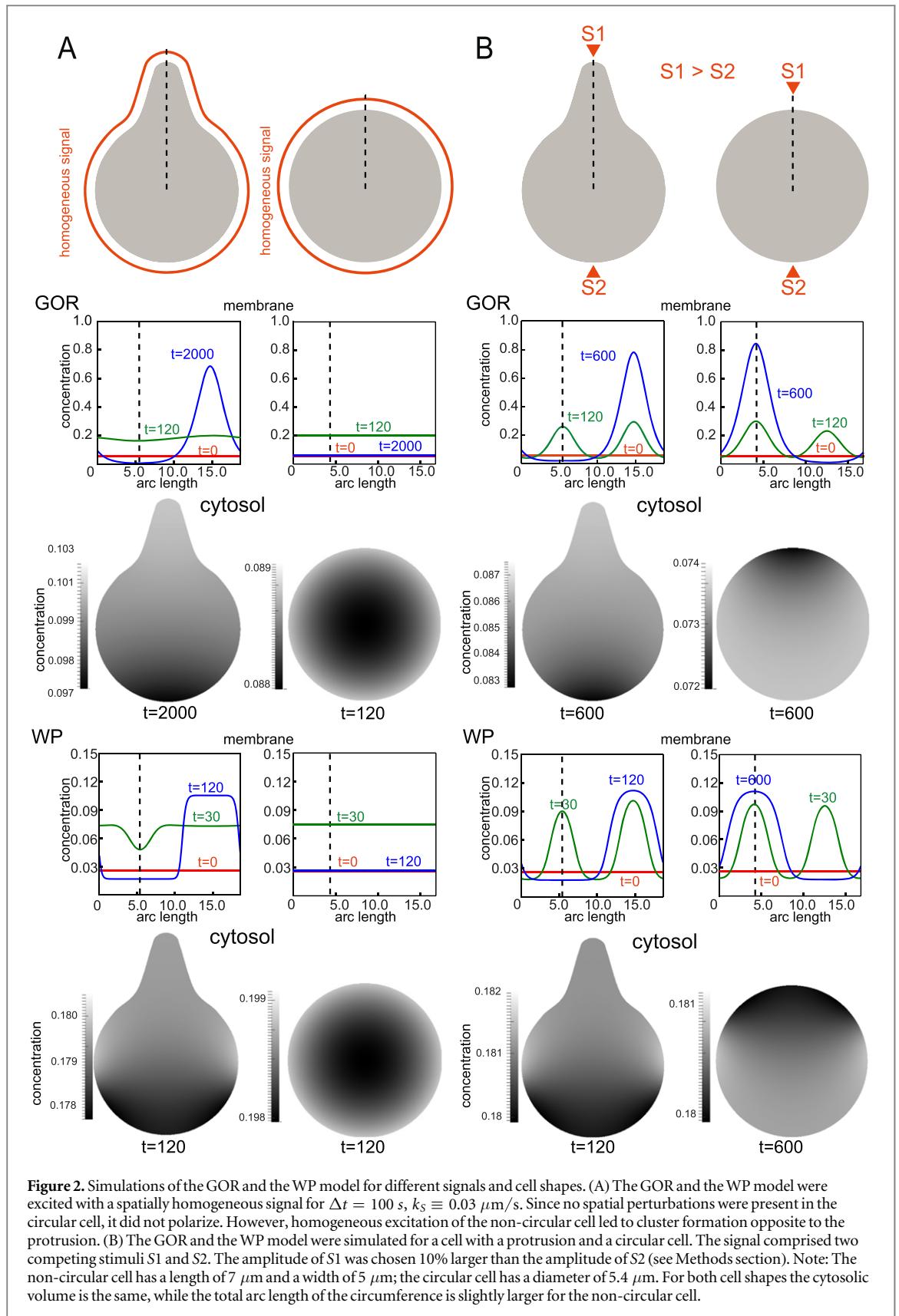
In [14], for instance, the membrane diffusion coefficient $D_m^{\text{GOR}} = 0.0025 \mu\text{m}^2/\text{s}$ was used, while in [15, 46] a 15-fold larger value $D_m = 0.037 \mu\text{m}^2/\text{s}$ was employed for the same model organism yeast. However, in this work it is not our aim to resolve reported parameter variations, or different modeling choices, but to illustrate systematically that the behavior of two common RD-based polarization models can be dramatically influenced by cell shape and diffusion inhomogeneities. In the experiments shown in this work, we thus simulated both models with a set D_m^{cons} of consensus diffusion coefficients which are approximately the geometric mean of extreme values of diffusion coefficients found in the references (see table 2).

To get a first impression of our higher dimensional formulation of the GOR model and the WP model, it is reasonable to perform 1D simulations of the original models and comparable 2D simulations. We employed a fully circular cell without any inhomogeneities for the 2D simulations. It could be shown that both higher dimensional models are capable of qualitatively reproducing the 1D simulations which are performed in review article [16] with parameters given therein. A comparison of 1D and 2D simulations with two competing stimuli, for example, can be found in figure S3 in supplementary material S1.

In silico experiments

(A) Protrusions in a cell locally limit molecule aggregations

In a first setup, we strive to understand the influence of the cell shape on the polarization behavior by the introduction of a protrusion to an otherwise fully circular cell. In [19], it was shown that the cell shape potentially influences signaling within the cell for one cytosolic species, neglecting the membrane-cytosol shuttling. In a computational study [25] for models of motile cells like neutrophils or *Dictyostelium*, the polarization was also examined in the case of a static geometry. For an elliptical geometry, cells repolarized along the major axis when initially polarized along the minor axis without further stimulus or bias. For the MinCDE system, a similar effect was observed in a model with membrane-cytosol coupling and an elliptical cell shape [49]. There, pole-to-pole oscillations of Min proteins predominantly occurred along the major



axis as well. However, for a non-oscillatory polarization model as used in our study and a more complex geometry, it was not obvious what effect to expect. In the following experiments, we incorporate a protrusion into a circular cell as shown in figure 2. The cell shape is motivated by the shape of a yeast cell during

mating with the protrusion representing a mating projection. However, similar shapes can also be found in other cell types like dendritic spines [50].

First, a homogeneous signal was employed to excite the cell from its resting homogeneous steady state. Using the mechanism introduced in

equation (9), the signal $k_S \equiv 0.03 \mu\text{m}/\text{s}$ was applied for a time period of $\Delta t = 100 \text{ s}$ on the surface of a circular cell with a diameter of $5 \mu\text{m}$ and a cell which has a protrusion with length $2 \mu\text{m}$ (see figure 2(a)). As expected, the circular cell did not polarize since there were no asymmetries in the signal or in the cell shape. Once the signal vanished, the cell returned to its unexcited resting state. For the non-circular cell, we observed a different effect. A flux was induced from the cytosol to the membrane. This created a cytosolic gradient from the protrusion (lower concentration) to the opposite side of the cell (higher concentration) since the ratio surface to volume was larger in the protrusion than in the circular part. The concentration of the surface constituent, therefore, also grew faster on the opposite side of protrusion. Due to the positive feedback, the concentration gradient on the surface was amplified and a unique cluster was established. The positive feedback in both models also led to a dramatically reduced concentration of inactive molecules in the cytosol which reverses the cytosolic gradient (shown in figure 2(a)). The membrane-cytosolic flux was still positive in the cluster region but negative elsewhere. The geometry effect was more pronounced for the WP model where polarization was established very fast (less than 100 s) while the GOR model polarized much slower ($\sim 1000 \text{ s}$).

Second, we imposed a signal comprising two stimuli S1 and S2 on the cell surface. The stronger stimulus S1 was located at the protrusion while the weaker stimulus S2 was located at the opposite side of the cell (see figure 2(b)). For the circular cell, we observed the expected outcome: the stronger stimulus S1 induces a cluster of active membrane-bound molecules which dominated the smaller cluster induced by S2. Eventually, the smaller cluster vanished and the system reached a polarized steady state for both models. However, we observed that the protrusion reversed the outcome. As in the former setup with a homogeneous signal, the cytosolic concentration decreased faster in the protrusion and therefore limited the cluster growth at the site of S1. Eventually, the cell was oriented toward the opposite side of the protrusion.

The effect that we observed in the simulations can be described as a kind of ‘bottle neck’ caused by the protrusion at the site of S1. In particular, diffusive transport into the protrusion was slightly hindered when compared to diffusion on the unperturbed membrane. Thus, the location with the stronger stimulus S1 at the protrusion was not able to ‘win the competition’ against the initially smaller cluster at the site of S2 due to insufficient transport of inactive signaling molecules to the site of S1. This effect might be interpreted in the context of the narrow escape problem [50]. The emerging cluster acts as an absorber of cytosolic molecules since there is a flux from the cytosol to the membrane at the emerging cluster. The

mean time for a molecule in the cytosol to reach the cluster (or absorber) is greater at the protrusion than in the circular part of the cell surface. Slow cytosolic diffusion or narrowing of the protrusion increases the mean time and, hence, slows down molecule aggregation in the protrusion. For analytical results of the narrow escape time applied to dendritic spines, we refer to [51].

In [30], we stimulated yeast cells with pheromone where yeast cells formed protrusions toward a spatial gradient. When the gradients were almost uniform or the gradients were perturbed by small rapid changes, the yeast cell still polarized and grew a protrusion several times, but not in the same direction. This effect has also been observed in other experimental works for yeast [52–54]. Moreover, in experiments with *Dictyostelium* cells and neutrophils it was reported, that unless gradients were very steep, new pseudopods steered cells away from the direction of the old pseudopod [55]. In a dynamic cell shape model [29], the effect was explained by the dilution of the activator by surface expansion of the cell surface in the pseudopod region. Our study suggests that this effect can alternatively be explained by a narrowing of the volume that occurs when a pseudopod is extended.

Based on these observations, we complemented our simulations with stimuli that act as gradients on the cell surface. Again, the protrusion acted as a negative feedback and even if the protrusion was aligned toward the gradient, the polarization occurred on the opposite side of the cell if the gradient was very shallow (see figure S7 in supplementary material S1). This demonstrated nicely that small perturbations in the cell shape may lead to a qualitative difference in the behavior of both models. One interpretation of this observation is that the growth of a protrusion evokes a direct feedback on the underlying biochemical process, i.e. spatial geometrical changes cause changes in the biochemical properties of signaling pathways. This effect might be a generic feature of cell polarization that damps spurious deformations and promotes reorientation in case of ambiguous signals.

(B) There is an optimal cell size for polarization

In the previous experiments in (A), we simulated a cell with constant diameter of $5 \mu\text{m}$. A variation of the cell’s diameter directly determines the distances that molecules have to travel within the cell. For instance, the mean square displacement of a molecule in the cytosol in some time interval Δt can be calculated from $4D_c \Delta t$ for unconstrained 2D diffusion. Assuming a diffusion coefficient in the range $1 \mu\text{m}^2 - 10 \mu\text{m}^2$ [11, 16, 56], we can conclude that the root-mean square distance $\sqrt{4D_c \Delta t}$ varies between $2 \mu\text{m} - 6.32 \mu\text{m}$ in a time interval of $\Delta t = 1 \text{ s}$. For a small cell with a diameter of $3 \mu\text{m}$, which can be

assumed for small yeast cells, this means that one molecule typically travels from one end of the cell to the other in less than one second. It thus is apparent that passive transport processes are much more efficient in small cells than in larger volumes. However, higher concentration differences as well as multi-directional gradients that interfere with each other are expected in larger cells.

There are several mathematical approaches for the analysis of RD models. These can be used to obtain parameter studies of crucial model parameters such as cell size, initial conditions kinetic parameters and diffusion coefficients. A classical method is linear stability analysis (LSA) which was performed in [15, 57, 58] for bulk-surface RD systems. In this approach, the equations are linearized around a homogeneous steady state and the polarization behavior of the model is studied in the linear regime. There is also a more recent approach called local perturbation analysis [59, 60] which characterizes the nonlinear regime and reduces complex reaction-diffusion equations to a small set of ordinary differential equations. However, the analysis is based on the assumption of very fast cytosolic diffusion coefficients (e.g. $D_c \rightarrow \infty$) and very slow diffusion coefficients on the membrane (e.g. $D_m \rightarrow 0$) and, hence, the interdependence of fast and slow diffusion is not investigated. Therefore, we performed the classical LSA which was complemented with numerical simulations in the nonlinear regime. We point out that there is also a possibility to extend the LSA into the nonlinear regime [45], however, this analysis goes beyond the scope of this study and could be addressed in future studies.

In the following analysis, we consider circular cells of radius R . The surface constituent u was decomposed into a Fourier series with summands $\exp(\lambda_k) \cos(k\phi)$ and $\exp(\lambda_k) \sin(k\phi)$, where k is the wave number and λ_k the corresponding growth mode. The volume constituent was expanded into a series using the fundamental solutions for the radial part, i.e. modified Bessel functions of the first kind (see supplementary material S1 for details). The fundamental solutions for both the surface and the volume constituent are shown in figure 3(a) for different wave numbers k . Note that the wave numbers $k \geq 1$ correspond to the number of polarization sites of the cell. We derived an analytical expression for the corresponding growth modes λ_k . These are depicted in figure 3(b) in dependence on the cell size. For larger cell sizes, multiple peaks become unstable, while for small cells all λ_k are negative and, therefore, no polarization occurs in the linear regime. A phase portrait for the influence of cytosolic and membrane diffusion coefficients is shown in figure 3(d). To get an understanding of the interplay of positive feedback, cell size and diffusion coefficients, the following estimate for λ_k was derived:

$$\begin{aligned} & f_u(\bar{u}_0, \bar{v}_0 |_{r=R}) \\ & - \frac{D_m k^2}{R^2} - \frac{f_u(\bar{u}_0, \bar{v}_0 |_{r=R}) f_v(\bar{u}_0, \bar{v}_0 |_{r=R})}{\frac{D_c k}{R} + f_v(\bar{u}_0, \bar{v}_0 |_{r=R})} \\ & \leq \lambda_k \leq f_u(\bar{u}_0, \bar{v}_0 |_{r=R}) - \frac{D_m k^2}{R^2}, \end{aligned} \quad (13)$$

where (\bar{u}_0, \bar{v}_0) denotes a steady state of the system (see Text S1 for a derivation). For large cytosolic diffusion coefficients D_c , the term (*) is very small and the approximation $\lambda_k \approx f_u(\bar{u}_0, \bar{v}_0 |_{r=R}) - D_m k^2 / R^2$ can be used. From this approximation it can be seen immediately how the membrane diffusion rate D_m counteracts the positive feedback $f_u(\bar{u}_0, \bar{v}_0 |_{r=R})$ with respect to the membrane concentration. It follows that for small cell sizes $R_- < \sqrt{\frac{D_m}{f_u(\bar{u}_0, \bar{v}_0 |_{r=R})}}$ there are no growing eigenmodes and, hence, no spontaneous cluster formation takes place. However, for cell sizes $R_+ > 2 \sqrt{\frac{D_m}{f_u(\bar{u}_0, \bar{v}_0 |_{r=R})}}$ there is more than one growing eigenmode and multiple transient polarization sites are possible. For the GOR model, we investigated the stable non-zero homogeneous steady state, while for the WP model, we investigated the transient homogeneous steady state (\bar{v}_0, \bar{u}_0^T) , where phase separation occurs.

In experiments [42], it was shown that over-expression of Cdc42 led to multiple polarization sites and the dependency on the GEF was reduced. Motivated by these experiments, we varied the total molecule number of signaling molecules with respect to the positive feedback mediated by its GEF. In the case of the GOR model, we varied the crucial parameter E_c and for the WP model the parameter γ as shown in figure 3(c). The steady state (\bar{u}_0, \bar{v}_0) for the stability analysis depended on changing E_c and γ for the GOR and WP model, respectively. The number of molecules was deduced from the mass of the steady state as given in equation (10) by assuming a slice of the cell with height $1 \mu\text{m}$. For the GOR model, we observed the expected effect that higher molecule numbers led to multiple clusters. Furthermore, polarization occurred already for a slow positive feedback E_c if the molecule number was high. For the WP model, there was an upper bound for the molecule number that led to polarization. Here, a strong positive feedback led to a wider range of molecule numbers. For further analysis of the WP model, we refer to [47].

Simulations for circular cells with cell diameters in the range of one order of magnitude from $1.5 \mu\text{m}$ up to $15 \mu\text{m}$ were performed to demonstrate the behavior of both models in the nonlinear regime. For all cell sizes, we first imposed one single stimulus and second two conflicting stimuli S1 and S2 on the cell membrane. The amplitudes of the stimuli were fixed while the membrane areas of the stimuli were scaled proportionally to the cell size to make simulations with

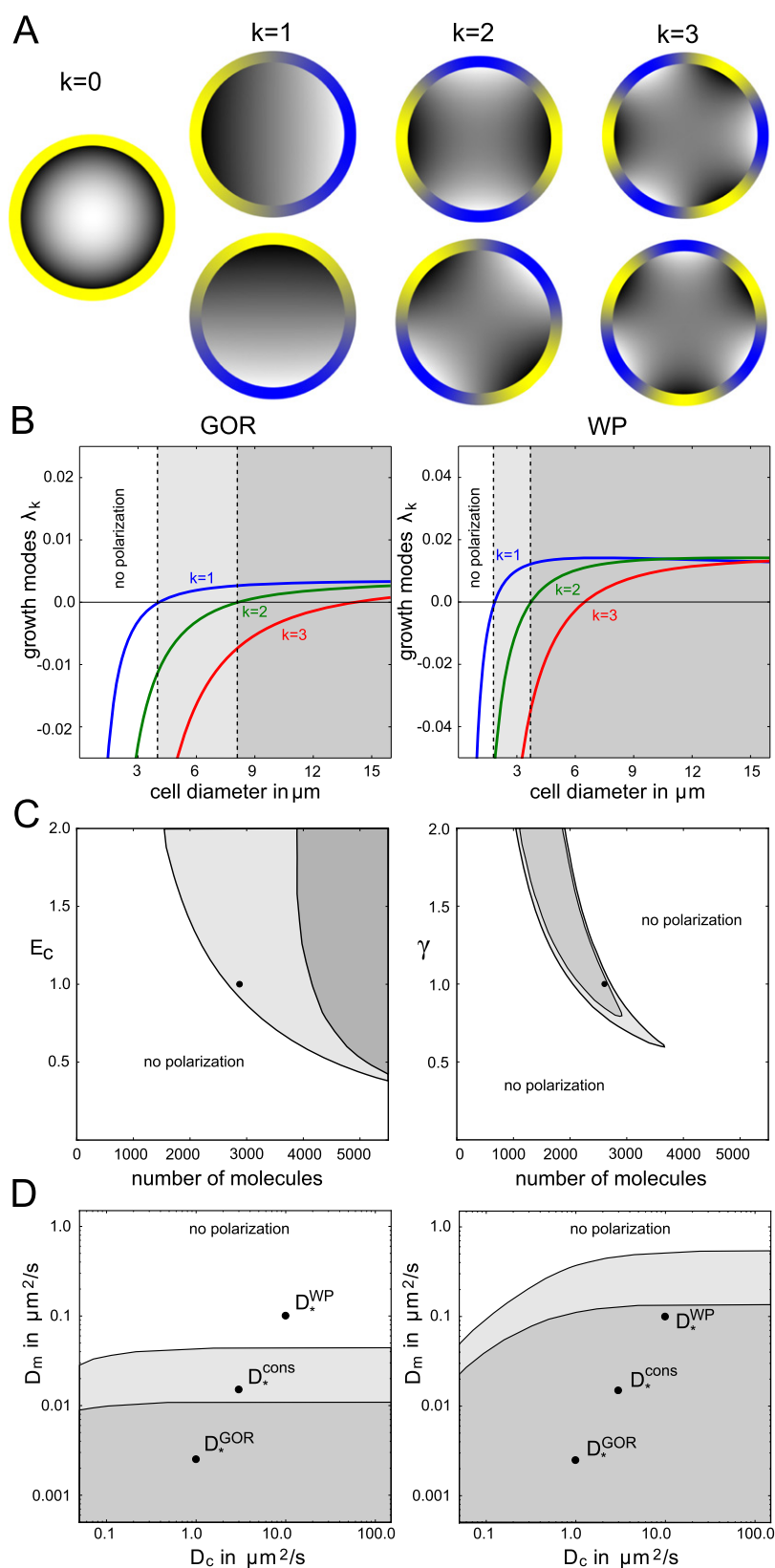


Figure 3. Parameter study based on linear stability analysis. (A) Schematic illustration of the fundamental solutions for different wave numbers k . Here, high and low concentration on the membrane is indicated by yellow and blue, respectively. High and low concentration in the cytosol is indicated by light gray and dark gray, respectively. (B) Dependence of growth modes on the cell size. If all growth modes are negative (white region), the homogeneous steady state is stable. In case $\lambda_1 > 0$ and $\lambda_2, \lambda_3 < 0$ (light gray region), exactly one cluster emerges. If also $\lambda_2 > 0$ or $\lambda_3 > 0$ (dark gray region), multiple transient polarization sites can occur in the linear regime. (C) Phase portrait of positive feedback and total molecule number variation in a slice through the cell of height $1 \mu\text{m}$. (white: no polarization; light gray: exactly one cluster; dark gray: multiple transient clusters possible). (D) Interdependence of polarization behavior and diffusion coefficients (same color coding as in (B) and (C)). Black dots show the extreme values used in the literature [10, 11].

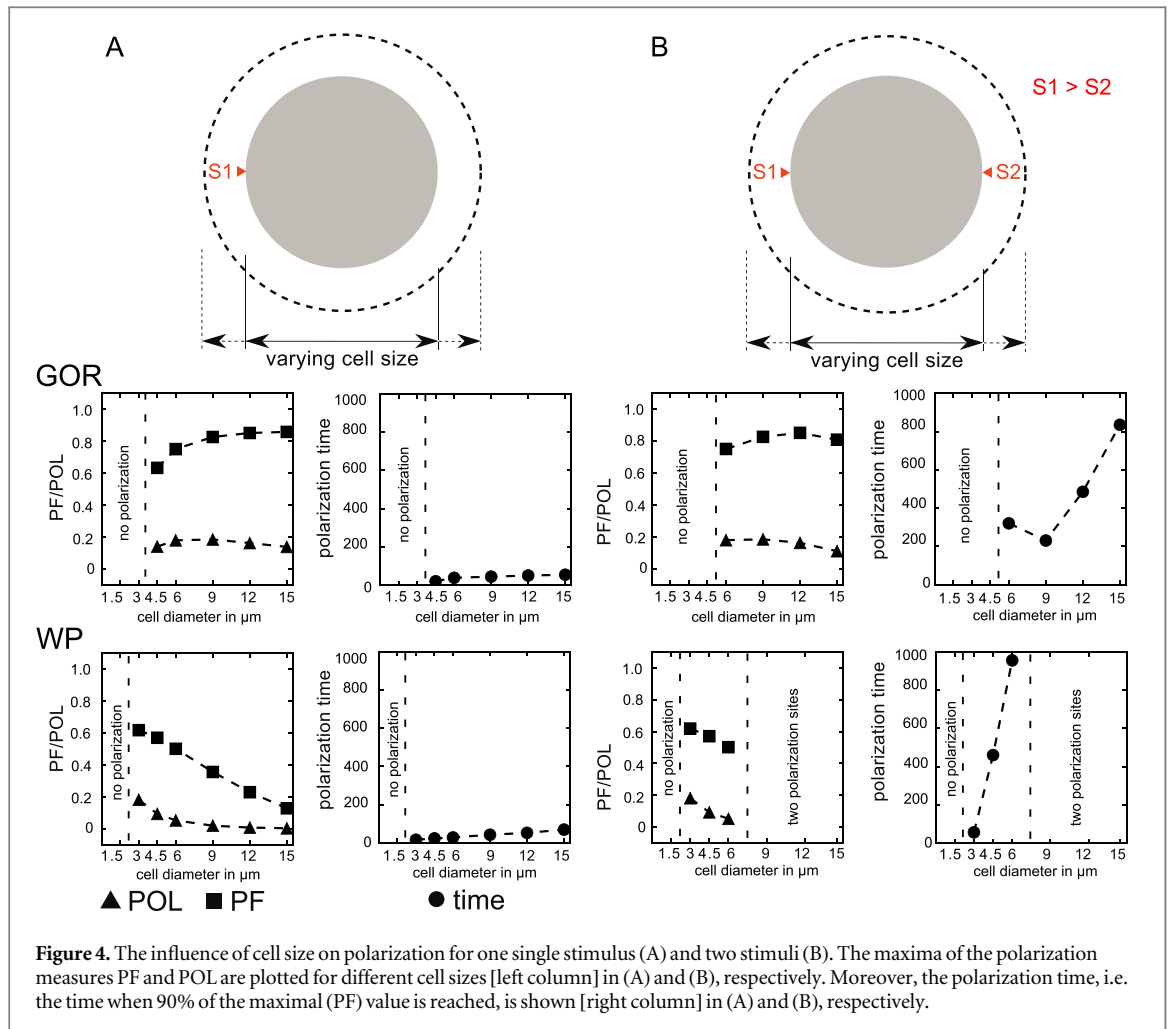


Figure 4. The influence of cell size on polarization for one single stimulus (A) and two stimuli (B). The maxima of the polarization measures PF and POL are plotted for different cell sizes [left column] in (A) and (B), respectively. Moreover, the polarization time, i.e. the time when 90% of the maximal (PF) value is reached, is shown [right column] in (A) and (B), respectively.

different diameters comparable. In general, two clusters emerged and competed with each other. It is of interest which influence the cell's diameter has on this competition.

In order to evaluate the influence of cell size, we introduced two measures to compare the degree of polarization on the membrane (see Methods section). The first was the mean polarization (POL) which related the highest concentration to the total mean concentration on the surface normalized by the surface area. The second was the polarization factor (PF) which was calculated from the area of the smallest surface patch that comprised half of the mass on the surface. For the steady states of the simulations, we calculated PF and POL for varying cell sizes, see figure 4.

The GOR and WP models exhibited essentially different polarization behaviors. For the GOR model, the clusters grew mainly in 'height' (i.e. locally high concentrations), while for the WP model a traveling wave could be observed where the cluster grew in width but not in height.

For the GOR model, we observed that the POL measure slightly decreased, since the cluster height did not grow proportionally to the cell diameter (compare figure 4). On the other hand, the relative cluster width

was decreasing and therefore the PF measure was increasing with cell size. The development of the relative cluster width in relation to the cell size is shown in figure S5 in supplementary material S1. It should be noted that for a cell with a diameter smaller than $4.5 \mu\text{m}$, polarization was not achieved for the employed parameters.

For the WP model, the POL measure decreased with increasing cell size since the cluster height was the same for smaller and larger cells. The PF measure decreased as well. The surface to volume ratio scales with $2/R$. Hence, if the maximum concentration of the cluster is fixed, the cluster width grows with cell size. An explicit formula for the cluster width is derived in supplementary material S1. The formula was in almost exact agreement with the numerical 2D simulation and predicts that the relative cluster grows linearly with R . For a cell with a diameter of $15 \mu\text{m}$, more than 80% of the cell surface was polarized (see figure S6 in supplementary material S1). For a cell with a diameter smaller than $3 \mu\text{m}$, polarization was not achieved in the case of one and two stimuli. In the case of two stimuli at opposite sites, no steady state was reached in a time frame of less than $t = 2000 \text{ s}$ for a cell with a diameter larger than $6 \mu\text{m}$.

We also compared the duration for the build-up of polarization by measuring the time until 90% of the final PF value was reached. The increase for larger cells was especially significant. In case of one single stimulus, we observed an increase from 21 s for a cell with diameter 4.5 μm to 55 s for a cell with diameter 15 μm for the GOR model. For the WP model, we observed an increase from 17 s (cell diameter 3 μm) to 80 s (cell diameter 15 μm). Much more pronounced was the increase in case of two stimuli. In fact, for the WP model the polarization time increased from 43 s (cell diameter 3 μm) to 953 s (cell diameter 6 μm) and a single site of polarity was not established within 2000 s for cells with a diameter larger than 6 μm . For the GOR model, the polarization time for a cell with diameter 15 μm more than doubled compared to a cell with diameter 6 μm .

For both models, we observed that polarization is either not possible for very small cells or takes very long for larger cells. Regarding the chosen parameter values, we could demonstrate that there is indeed an optimal cell size for both mechanisms.

(C) Membrane barriers can amplify cluster formation

Interior subdomains such as organelles and diffusion barriers on the membrane potentially play an important role in the signaling process. In budding yeast, bud and birth scars occur after cell division and may influence subsequent cell polarization. Furthermore, it is known that during cell division diffusion barriers are established to separate material of mother and daughter cells while they still share a contiguous membrane [61–63]. In a recent study [14], it was shown that septin structures in yeast are formed in the early phase of polarization and that Cdc42 clusters can be trapped in these regions. Furthermore, septins also play an important role in steering the direction during chemotropic growth [52]. We introduced membrane diffusion barriers into the model to examine the influence of these inhomogeneities on polarization behavior, see figure 5.

As in the previous setups, a signal comprising two stimuli $S1$ and $S2$ was applied on the cell surface, but this time with the same magnitude to compare the effect of cell shape with the effect of slow membrane diffusion (see figure 5(a)). The cell geometry was exactly the same as in section (A). First, we simulated the effect of diffusion barriers surrounding the location of stimulus $S1$ (see left column in figure 5). Interestingly, the cluster induced by $S1$ grew steadily while the cluster induced by $S2$ vanished. Hence, the diffusion barriers compensated for the negative feedback caused by the protrusion as examined in (A). A similar effect was observed when applying a gradient on the cell surface. Again polarization was enhanced for both models. For the WP model the steady state was almost the same but was achieved in a shorter time frame. The

effect was much more pronounced for the GOR model. Here, polarization was only achieved with added diffusion barriers.

This effect can be attributed to an accumulation of signaling molecules at the site of $S1$ since the transport away from $S1$ is blocked by the introduced barriers.

We repeated the same setup with the same parameters and cell shapes. However, this time we employed only one single diffusion barrier which was placed next to stimulus $S1$ at the protrusion, see center column in figure 5. In yeast cells, such impermeable regions on the membrane corresponded to septin structures or bud scars which emerged after cell division. It is a topic of current research how septin structures influence the budding process and chemotropic growth. For the GOR model, we observed that due to restricted diffusion caused by the barrier, the cluster at the weaker stimulus $S1$ grew much stronger than the cluster at $S2$. We thus had the same effect as for surrounding diffusion barriers. However, the influence of a single diffusion barrier on one side was weaker. In the case of the WP model, it could not compensate for the negative feedback induced by the protrusion. For the GOR model, we observed that the direction of polarity moved toward the diffusion barrier, an effect that was used to explain the occurrence of bending shmoo during chemotropic growth of yeast cells [52]. The effects of barriers surrounding the protrusion and impermeable regions in the vicinity of the signal were qualitatively similar. During cluster formation on the membrane, active membrane-bound molecules diffuse laterally from high concentrations to low concentrations with diffusion coefficient D_m . The effect of diffusion barriers introduced in a 2D model as shown in this work can be different from those in a 3D model, since in 2D diffusion barriers block diffusion while in 3D there are more possible shapes of barriers. For example in 3D a ring shaped diffusion barrier around the neck of the shmoo is more constraining than a spot-shaped or circular diffusion barrier at the side of the shmoo. However, in both cases 2D and 3D, reducing the diffusion diminishes the diffusive flux which counteracts the growth of the cluster. Therefore, diffusion barriers on the membrane have the potential to accelerate, stabilize and steer cell polarization.

(D) Organelles in the cytosol can alter polarization preferences

Cells accommodate many structures of different sizes, for instance large membrane structures like the endoplasmic reticulum, the nucleus and other organelles. Thanks to recent advances in imaging technologies, very detailed microscopic images of the cytoplasm can be produced, see for example [2, 3, 64]. Intracellular structures certainly influence diffusive but also vesicular transport in the cell [35, 65, 66]. During cell division, the spatial position of the organelles has to be organized and is most likely

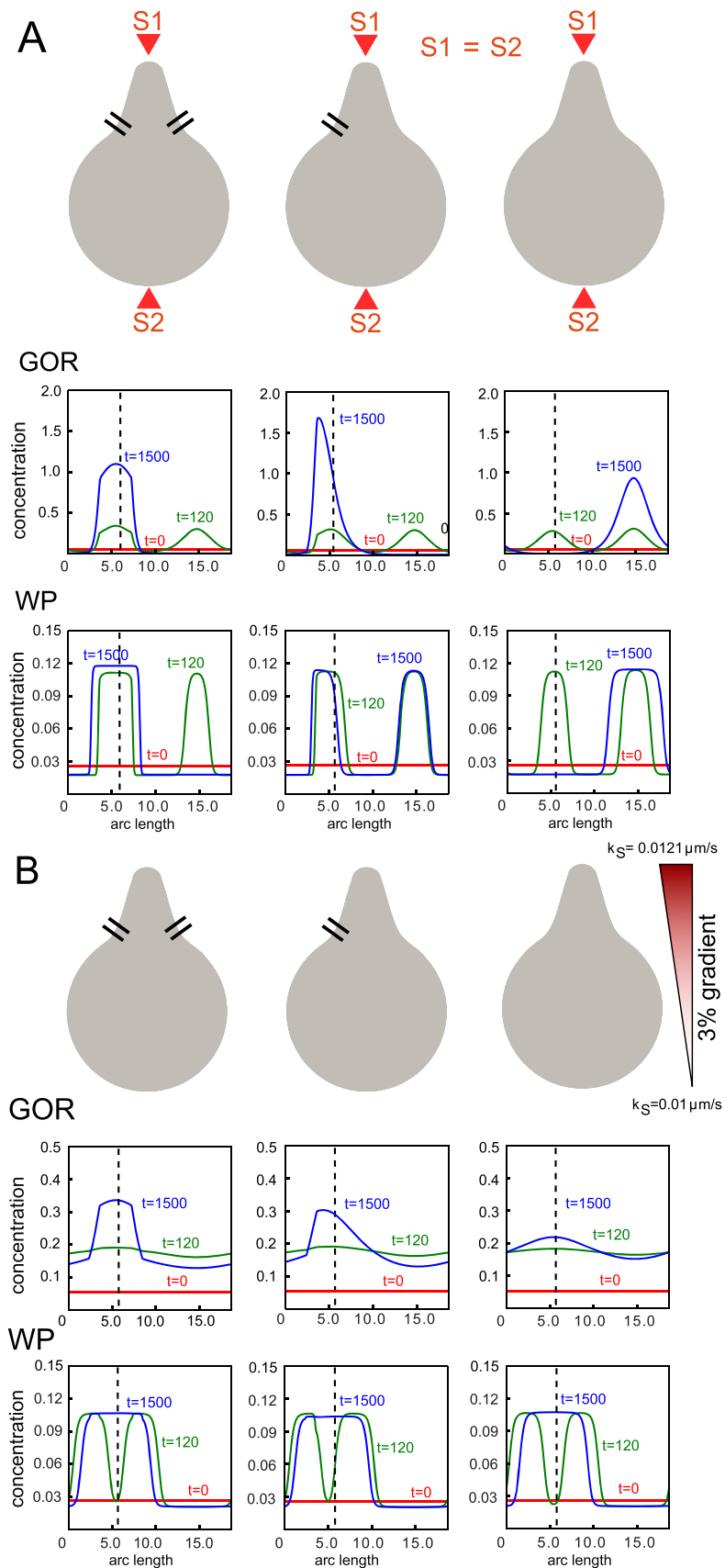
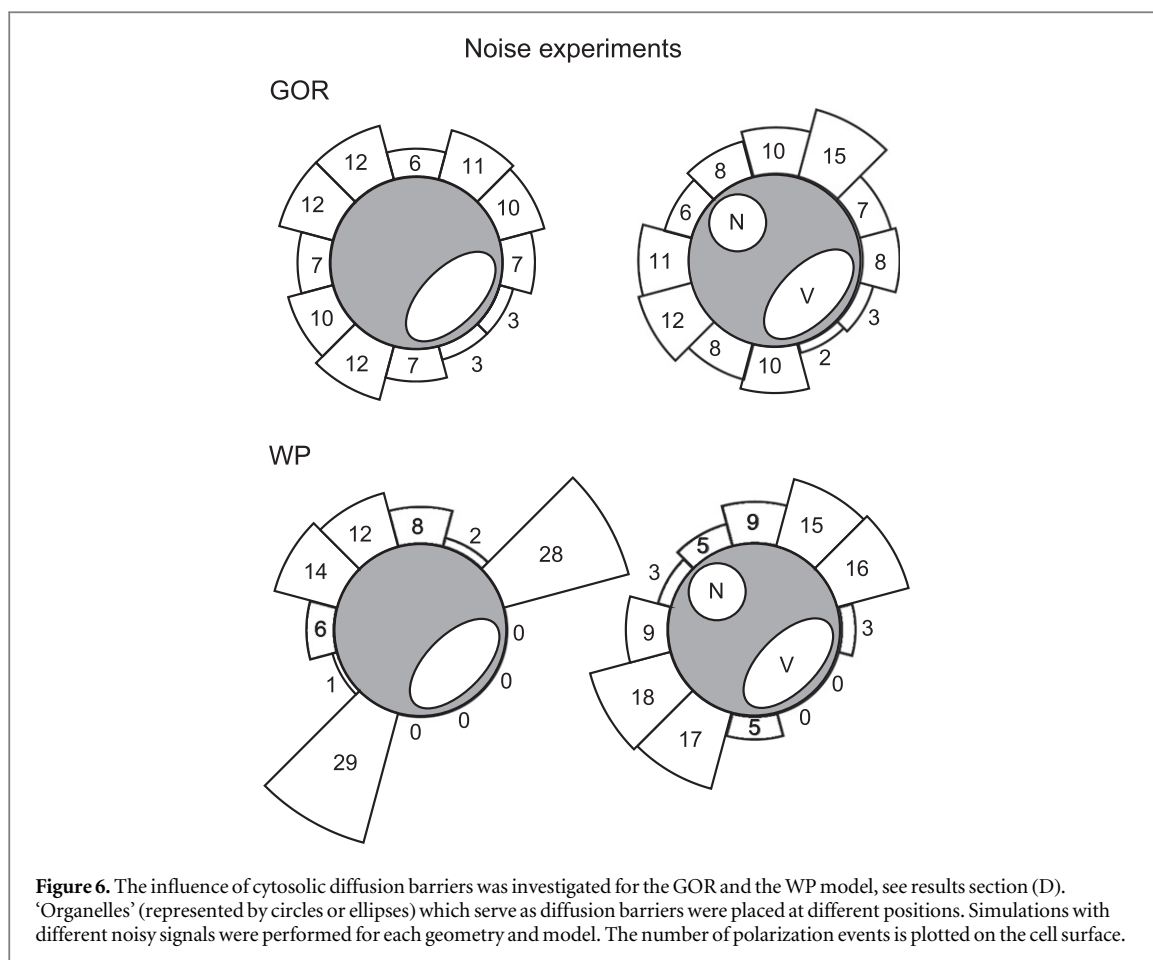


Figure 5. The influence of diffusion barriers on the membrane was investigated for the GOR and the WP model. (A) In contrast to section (A), the stimuli S1 and S2 were chosen equally strong in order to compare the influence of the shape with the effect of the barriers. Two diffusion barriers with 10-fold slower membrane diffusion were placed around the location of stimulus S1 [left column]. A single barrier with 10-fold slower diffusion was placed at the left-hand side next to the location of stimulus S1 [center column]. (B) A graded signal was used to trigger cell polarization. Again we examined two diffusion barriers [left column], one diffusion barrier [center column] and no barrier for comparison [right column].



controlled by signaling, but effectively also influences signaling itself [67]. Even for small cells, the calculation of effective diffusion coefficients usually is inferred from molecule properties and viscosity of the medium. However, these derivations do not incorporate intracellular diffusion barriers such as organelles or impermeable membranes in general. Therefore, we examined the effects of obstacles in the medium on intracellular gradients.

To address this goal, we performed computational experiments with organelles of different size and shape. In a first setup, we placed a large organelle with elliptical shape in the vicinity of the membrane. In a second setup, we added a smaller circular obstacle opposite to the large organelle near the membrane. In each case, a vast number of simulations with different noisy signals on the cell membrane was carried out. To assess the influence of the organelles, the cell surface was divided into twelve equal parts. For each simulation, the observed steady state polarization direction was assigned to the respective part in order to obtain a likelihood distribution of preferred polarization sites, see figure 6.

The effect of the large organelle is very clear and polarization close to the organelle turned out to be very unlikely for both models WP and GOR. In 100 simulations for each setup and model, at most 3 polarization events could be observed in one of the

segments next to the organelle for the GOR model and 0 for the WP model. However, in a circular cell without diffusion barriers, the expectation value of polarization events for each area segment is $100/12 \approx 8.3$. A similar but much less pronounced effect was induced by the small circular organelle. In particular, an interesting pattern could be observed for the WP model. Most polarizations occurred in the neighborhood of (but not behind) the large organelle or at the opposite side. This can be explained by the complex cytosolic gradients that form due to the cytosolic barriers. In case of polarization, the growing cluster acts as an absorber of cytosolic molecules. If aggregation occurs behind the organelle, an initial cluster is quite likely to vanish due to the limited transport. If polarization takes place further away from the organelle, molecule transport is hindered by the organelle and a cytosolic gradient toward the organelle is formed which leads to a movement of the cluster toward the organelle. This effect was much more pronounced for the WP model but it could also be observed for the GOR model. To complement the experiments, a deterministic investigation of the effect for organelles of different sizes is shown in figure S4 (in supplementary material S1).

We conclude that the GOR model is more gradually influenced by the shape of the organelles in the cytosol, while the steady state of the WP model

behaves rather like a switch with respect to the introduction of different cytosolic diffusion barriers.

Discussion

Cell polarization is a fundamental process during cell division, cell differentiation and directed growth. In this paper, we focused on the crucial initial phase of polarization when a polarization site is established. Since spatial aspects are often neglected in computational as well as experimental investigations, our main question was whether and how spatial parameters like cell size, cell shape and spatial inhomogeneities influence the polarization process.

Our study is based on a class of conceptual two component models which describe the shuttling of molecules from the cytosol to the membrane and vice versa. Various models of this type can be found in the literature. Since many of these models have been formulated and simulated only in a 1D environment, we suggest a consistent expansion of this class of models to 2D and 3D. In the framework presented in this study, different cell shapes, curved membranes, diffusion inhomogeneities and barriers were integrated. This allowed us to go beyond the variation of kinetic parameters to the introduction of several crucial spatial properties and their influence on the polarization process. For this, it is essential to perform simulations at least in 2D so that differences in surface to volume ratio, cell shape and organelles placed in the cytosol can be represented and taken into account.

In our study, we illustrated that the influence of cellular inhomogeneities can be quite dramatic and should certainly be considered in modeling and simulation of spatial intracellular processes. For the reaction kinetics, we chose the GOR model with a Turing-type mechanism on the one hand, and the WP model with a wave-pinning mechanism on the other hand. With these two kinetics, a vast number of computational experiments were carried out in order to examine the influence of (A) the cell shape, (B) the cell size, (C) inhomogeneities on the membrane and (D) organelles in the cytoplasm.

Importance for cell polarization in yeast

For the first setup (A), we illustrated that protrusions act as a negative feedback for both mechanisms, which led to a lower sensitivity to external signals in this region. In the presence of high pheromone concentration ($\approx 1\mu\text{M}$) for a long time period ($t > 2h$), yeast cells form multiple shmoos in distinct directions [30, 54, 68, 69]. The periodic formation of mating projections has been explained by a downregulation and termination of polarized growth mediated by Sst2 [68, 70], a regulator of G protein signaling (RGS). After termination of the growth of the first mating projection, the system polarizes again in the presence of high pheromone concentration. The second mating

projection forms in a distinct direction than the first one. It would be interesting to investigate experimentally whether the reorientation is mediated by a time delayed memory e.g. localization of Sst2 in the first mating projection, or by the geometry dependence of the Cdc42 polarization module as shown in this study.

Furthermore, we demonstrated in setup (B) that using fixed kinetic parameters there exists an optimal cell size for the GOR and the WP model. For both mechanisms, the polarization measured by the average polarization (POL) decreases for larger cells, while polarization times increase dramatically. Opposite to that, small cells were unable to polarize at all. We derived estimates for theoretical upper and lower bounds for the cell size depending on the kinetic parameters that control the positive feedback of Rho GTPase activation (see setup (B) or Text S1 for a derivation). It is an interesting question whether the size limits that hold for the theoretical models can be matched with experimental investigations in yeast. An experimental study on size dependent mating partner selection in yeast can be found in [71].

Diffusion inhomogeneities on the membrane are investigated in setup (C). We showed that diffusion barriers can act as a positive feedback on cluster formation. Diffusion on the membrane usually counteracts cluster formation. Hence, local obstruction of membrane diffusion yields an amplification of the signal. Diffusion barriers in yeast are mediated for instance by cytoskeletal scaffolding proteins known as septins. A recent experimental study [52] investigated the interplay of septins and the turning of the polarization cap in life cell imaging upon stimulation with low pheromone concentration. The authors could show that the probability of turning the Cdc42 polarization cap in a short time scale of a few minutes is limited for wild type cells, where the septins form at the edge of the polarization cap. However, deleting the Sst2 resulted in cells, where the polarization cap wandered along the cell periphery and cells failed to grow persistently.

The behavior of the WP model for gradient tracking on short time scales, which is not a feature of the GOR model, might be more suitable to explain the mutant behavior of *sst2Δ* cells. However, with diffusion barriers both models seem to behave roughly the same, e.g. cluster formation is promoted and stabilized by septins. Both setups (A) and (C) encourage further investigation of the temporal and spatial localization of septins and RGS proteins like Sst2. We point out that diffusion barriers induced by the cytoskeleton can also be modeled as local energy barriers that modulate the obstacle strength dynamically. A model describing the interplay of slow diffusion induced by the cytoskeleton and active transport was investigated in [72], which could be a useful approach for mating and budding yeast as well.

In experimental setup (D), we introduced different organelles into the cytosol. We illustrated that reduced transport due to obstacles led to a change of the

polarization behavior despite fast cytosolic diffusion. In particular, placing an organelle in the vicinity of a cluster limited the membrane-cytosolic shuttling and, therefore, also limited the possible growth of the cluster. We observed that the WP model was more sensitive to obstacles and organelles than the GOR model. We suggest that cell polarity and the organization of organelles should be investigated in two directions; experimentally, by observing the orchestration of molecule aggregations and the positioning of organelles [64]; computationally, by incorporating active transport and the cytoskeleton as suggested in [59, 73]. However, the incorporation of the effect of inclusions and organelles in a comprehensive model with active transport and cytoskeleton has to be addressed in future research.

Outlook and relevance for other organisms

The results of this paper are based on static geometries which can be assumed for the initial establishment of polarization or for cells that grow slowly in comparison to the diffusion and polarization processes. These assumptions are valid for many fungi, but also plant cells or neurons. Apart from this, the observation that spatial inhomogeneities may significantly influence intracellular transport processes is generically applicable to most cells and requires further research. For instance, we believe that our approach could be beneficially embedded in forward-looking multiphysics frameworks as presented in [74] or [59], where deformable cell geometries are combined with signaling on the cell membrane.

The application of our approach for spatial modeling and simulation in a 3D setting is obvious since it only needs straightforward reformulation. We expect the influence of the cell shape to be even stronger in 3D. As in the 2D results, the local ratio of membrane and cytosol volume will be a key to characterize the influence of the cell shape. Therefore, we expect cluster emergence to preferentially occur in regions of minimal mean curvature in case of a uniform or noisy signal as also hypothesized in [10].

In the case of migratory cells such as neutrophils, fibroblasts or *Dictyostelium discoideum*, the underlying mechanism differs from yeast. Here, it is well-known that phosphatidylinositol-3,4,5-trisphosphate (PIP3), a membrane lipid that promotes Rho GTPase activation, increases sensitivity at the pseudopods through active transport. However, in experiments with *Dictyostelium discoideum* and neutrophils it was shown that the leading edge of the pseudopod splits into two and the new pseudopod steers the cell away from the direction of the old pseudopod [55]. In a theoretical study [29] this effect was explained by the dilution of signaling molecules on the cell surface due to surface expansion. Our study motivates two other possibly explanations. First, we clearly expect that narrowing and extending the leading edge increases the surface to

volume ratio locally and limits the recruitment of molecules onto the cell surface. Second, we suggest that extending the volume in a dynamic geometry causes a dilution of signaling molecules in the cytosol.

Recent advances in imaging techniques such as TIRF as well as confocal and electron microscopy have the potential to provide quantitative data for the spatio-temporal organization of cellular structures and spatial inhomogeneities. Computer tomographic images of cells can be translated into computational meshes and could serve as a basis for spatial modeling and simulation using real cell data in the future.

Our results suggest many spatial effects that could be investigated with the aid of such methods. Therefore, we hope that our approach leads to experimental investigations that give more insight into fundamental processes such as cell differentiation, directed growth and cell division.

Methods

Signal repertoire

To qualitatively compare the influence of different spatial effects, the GOR and the WP models were excited and probed with different kinds of signals which are described in more detail in the following subsection.

1) Conflicting localized stimuli

In this setting, two different regions of the cell were excited simultaneously. The imposed signal comprises two localized stimuli and is given by

$$k_S(\vec{x}, t) = \begin{cases} S_1, & \text{if } t < t_1 \text{ and } \text{dist}(\vec{x}_{S_1}, \vec{x}) < w, \\ S_2, & \text{if } t < t_2 \text{ and } \text{dist}(\vec{x}_{S_2}, \vec{x}) < w, \\ 0, & \text{otherwise.} \end{cases} \quad (14)$$

Here, $\text{dist}(\vec{x}_1, \vec{x}_2)$ denotes the Euclidian distance between two points \vec{x}_1 and \vec{x}_2 and w specifies the width of the excited surface area. We excited the system with two competing stimuli at positions \vec{x}_{S_1} and \vec{x}_{S_2} on the cell membrane, where each stimulus covers 5% of the cell surface. We set different amplitudes for both stimuli, namely $S_1 = 0.44 \mu\text{m/s}$ and $S_2 = 0.4 \mu\text{m/s}$ in setup (A) as well as (B), and equal amplitudes $S_1 = S_2 = 0.4 \mu\text{m/s}$ in setup (C). Both stimuli were applied for a time period of $\Delta t = 10 \text{ s}$, i.e. $t_1 = t_2 = 10 \text{ s}$.

2) Graded signal

In this setting, the system was excited with a persistent graded signal in the x_1 - x_2 plane. It is defined by

$$k_S(\vec{x}, t) = c_0 + c_1 \cdot \left(x_2 - (\vec{x}_{min})_2 \right), \quad (15)$$

where \vec{x}_{min} is the lowest point along the x_2 -direction of the two-dimensional cell (opposite side of the protrusion). We used $c_0 = 0.01 \mu\text{m/s}$ and

$c_1 = 3.0 \cdot 10^{-5} \mu\text{m/s}$ in the experiments in setup (C), and $c_0 = 0.03 \mu\text{m/s}$ and $c_1 = 0 \mu\text{m/s}$ in setup (A).

3) External noise

The external noise used in setup (D) was assumed to be spatially uncorrelated. Thus, the noise at each location on the cell surface was generated by selecting independent and identically distributed stationary random variables at each time period $[t_1, t_2]$. This realization of the noise was then assigned to $k_S(\vec{x}, t)|_{t \in [t_1, t_2]}$. We tested a normal and a log-normal distribution with mean $\mu = 0$ and standard deviation $\sigma = 0.1$. The two distributions produced approximately the same results. The noisy signal was changed in time by regenerating $k_S(\vec{x}, t)$ each $\Delta t = 5 \text{ s}$.

Polarization measures

For a comparison of the models, we employed different polarization measures [12, 75] which provided an indication about the localization and strength of a polarization. The first measure is related to the largest value of the surface concentration which is denoted by $u_f = \max_{\vec{x} \in M^{\text{cell}}} u(\vec{x})$. For the comparison of varying concentrations, we define the average polarization by

$$\text{POL}(u) := \frac{1}{|M^{\text{cell}}|} \cdot \frac{u_f - \bar{u}}{\bar{u}},$$

$$\bar{u} := \frac{1}{|M^{\text{cell}}|} \int_{M^{\text{cell}}} u \, dA. \quad (16)$$

This measure gives us information on direction and magnitude of polarization. However, the size of the cluster and its relative mass is not reflected. To account for this information, we employed a second measure called the ‘polarization factor’. It is defined by

$$\text{PF}(u) := 1 - \frac{|M^+(x_f)|}{|M^{\text{cell}}|},$$

$$M^+(x_f) := \{\vec{x} \in M^{\text{cell}} : u(\vec{x}) > \bar{u}$$

$$\text{and } \|\vec{x}_f - \vec{x}\| < \rho\}, \quad (17)$$

where $\vec{x}_f \in M^{\text{cell}}$ such that $u_f = u(\vec{x}_f)$ and ρ is chosen small enough so that only the cluster around x_f is taken into account.

Numerical methods

Simulations were performed using the Distributed and Unified Numerics Environment (DUNE) [27, 76]. We used a conforming finite element method of first-order Lagrange elements on triangular meshes. The equation for the membrane-bound species was solved on the boundary of the mesh while the equation for the cytosolic species was solved in the entire meshed domain. The finite element meshes were generated with Gmsh [77]. All of our meshes comprise several thousand elements to guarantee a high precision of the simulation results, see the example meshes in figure S4

in supplementary material S1. More detailed information regarding the utilized numerical methods can be found in supplementary material S1.

Acknowledgments

This work was supported by a grant from the German Research Foundation (CRC 740 ‘From molecules to modules’) to EK, partly supported by a grant from the German Research Foundation (‘Mass-conservative coupling of bulk and surface processes on implicit, time-dependent domains’) to CE, and partly supported by the German Research Foundation (DFG EXC 1003 ‘Cells in Motion — Cluster of Excellence, Münster, Germany’).

References

- [1] Bakal C, Aach J, Church G and Perrimon N 2007 *Science* **316** 1753–6
- [2] Larabell C A and Nugent K A 2010 *Current Opinion in Structural Biology* **20** 623–31
- [3] Wei D, Jacobs S, Modla S, Zhang S, Young C L, Cirino R, Caplan J and Czymmek K 2012 *BioTechniques* **53** 41–8
- [4] Kukulski W, Schorb M, Kaksonen M and Briggs J A G 2012 *Cell* **150** 508–20
- [5] Mogilner A, Allard J and Wollman R 2012 *Science* **336** 175–9
- [6] Levchenko A and Iglesias P A 2002 *Biophys. J.* **82** 50–63
- [7] Ozbudak E M, Becskei A and van Oudenaarden A 2005 *Developmental Cell* **9** 565–71
- [8] Otsuji M, Ishihara S, Co C, Kaibuchi K, Mochizuki A and Kuroda S 2007 *PLoS Computational Biology* **e108** ISSN 1553-7358
- [9] Altschuler S J, Angenent S B, Wang Y and Wu L F 2008 *Nature* **454** 886–9
- [10] Mori Y, Jilkine A and Edelstein-Keshet L 2008 *Biophys. J.* **94** 3684–97 ISSN 00063495
- [11] Goryachev A and Pokhilko A 2008 *FEBS Letters* **582** 1437–43
- [12] Chou C S, Nie Q and Yi T M 2008 *PLoS ONE* **3** e3103
- [13] Chou C S, Moore T, Nie Q and Yi T M 2015 *Systems Biology, IET* **9** 52–63 ISSN 1751-8849
- [14] Okada S, Leda M, Hanna J, Savage N S, Bi E and Goryachev A B 2013 *Developmental Cell* **26** 148–61 ISSN 1534-5807
- [15] Klünder B, Freisinger T, Wedlich-Söldner R and Frey E 2013 *PLoS Computational Biology* **9** e1003396 ISSN 1553-7358
- [16] Jilkine A and Edelstein-Keshet L 2011 *PLoS Computational Biology* **7** e1001121 ISSN 1553-7358
- [17] Kondo S and Miura T 2010 *Science* **329** 1616–20
- [18] Kerszberg M and Wolpert L 2007 *Cell* **130** 205–9
- [19] Meyers J, Craig J and Odde D J 2006 *Curr. Biol.* **16** 1685–93
- [20] Odde D 2011 *Cell* **144** 325–6
- [21] Howard M 2006 *Curr. Biol.* **16** R673–5
- [22] Herant M and Dembo M 2010 *Biophys. J.* **98** 1408–17
- [23] Wolgemuth C W and Zajac M 2010 *J Comput Phys.* **229** 7287–308
- [24] Vanderlei B, Feng J J and Edelstein-Keshet L 2011 *Multiscale Modeling and Simulation* **9** 1420–43
- [25] Marée A F M, Grieneisen V A and Edelstein-Keshet L 2012 *PLoS Computational Biology* **8** e1002402
- [26] Cowan A E, Moraru I I, Schaff J C, Slepchenko B M and Loew L M 2012 *Methods Cell Biol.* **110** 195
- [27] Bastian P, Blatt M, Dedner A, Engwer C, Klöfkorner R, Ohlberger M and Sander O 2008 *Computing* **82** 103–19 ISSN 0010-485X
- [28] Holmes W R and Edelstein-Keshet L 2012 *PLoS Computational Biology* **8** e1002793
- [29] Neilson M P, Veltman D M, van Haastert P J M, Webb S D, Mackenzie J A and Insall R H 2011 *PLoS Biology* **9** e1000618

- [30] Diener C, Schreiber G, Giese W, del Rio G, Schröder A and Klipp E 2014 *PLoS Computational Biology* **10** e1003690
- [31] Li L, Gervasi N and Girault J-A 2015 *Nat Commun* **6**
- [32] Muñoz-García J, Neufeld Z and Kholodenko B N 2009 *PLoS Computational Biology* **5** e1000330
- [33] Hiraiwa T, Nagamatsu A, Akuzawa N, Nishikawa M and Shibata T 2014 *Phys Biol* **11** 056002
- [34] Schöneberg J and Noé F 2013 *PLoS ONE* **8** e74261
- [35] Ellis R J 2001 *Current Opinion in Structural Biology* **11** 114–9
- [36] Elf J and Ehrenberg M 2004 *Systems Biology IEE Proceedings* **1** 230–6 ISSN 1741-2471
- [37] Takahashi K, Arjunan S N V and Tomita M 2005 *FEBS Letters* **579** 1783–8
- [38] Vereb G, Szöllösi J, Matkó J, Nagy P, Farkas T, Vigh L, Mátyus L, Waldmann T A and Damjanovich S 2003 *Proc. Natl Acad. Sci. USA* **100**(14) 8053–8
- [39] Singer S J and Nicolson G L 1972 *Science* **175** 720–31
- [40] Elliott C M and Ranner T 2012 *IMA J. Numer. Anal.* drs022
- [41] Etienne-Manneville S 2004 *J Cell Sci* **117** 1291–300
- [42] Caviston J P, Tcheperegine S E and Bi E 2002 *Proc. Natl Acad. Sci. USA* **99**(19) 12185–90
- [43] Kofahl B and Klipp E 2004 *Yeast* **21** 831–50 ISSN 0749-503X
- [44] Meinhardt H 1999 *Journal of Cell Science* **112** (17) 2867–74
- [45] Rubinstein B, Slaughter B D and Li R 2012 *Phys Biol* **9** 045006
- [46] Freisinger T, Klünder B, Johnson J, Müller N, Pichler G, Beck G, Costanzo M, Boone C, Cerione R A, Frey E and Wedlich-Söldner R 2013 *Nat Commun* **4** 1807
- [47] Mori Y, Jilkine A and Edelstein-Keshet L 2011 *SIAM Journal of Applied Mathematics* **71** 1401–27
- [48] Walther G R, Marée A F M, Edelstein-Keshet L and Grieneisen V A 2012 *Bull. Math. Biol.* **74** 2570–99
- [49] Halatek J and Frey E 2012 *Cell Rep* **10** 741–52
- [50] Schuss Z, Singer A and Holcman D 2007 *Proc. Natl Acad. Sci. USA* **104**(41) 16098–103
- [51] Schuss Z 2012 *J. Sci. Comput.* **53** 194–210 ISSN 0885-7474
- [52] Kelley J B, Dixit G, Sheetz J B, Venkatapurapu S P, Elston T C and Dohlman H G 2015 *Curr. Biol.* **25** 275–85
- [53] Moore T I, Chou C S, Nie Q, Jeon N L and Yi T M 2008 *PLoS ONE* **3** e3865
- [54] Bidlingmaier S and Snyder M 2004 *Journal of Cell Biology* **164** 207–18
- [55] Andrew N and Insall R H 2007 *Nat. Cell Biol.* **9** 193–200
- [56] Brown G C and Kholodenko B N 1999 *FEBS Letters* **457** 452–4
- [57] Levine H and Rappel W J 2005 *Phys Rev E Stat Nonlin Soft Matter Phys.* **72** 061912
- [58] Rätz A and Röger M 2014 *Nonlinearity* **27** 1805
- [59] Edelstein-Keshet L, Holmes W R, Zajac M and Dutot M 2013 *Philos. Trans. R. Soc. Lond., B, Biol. Sci.* **368** 20130003
- [60] Holmes W R, Mata M A and Edelstein-Keshet L 2015 *Biophys. J.* **108** 230–6
- [61] Caudron F and Barral Y 2009 *Developmental Cell* **16** 493–506
- [62] Shlomovitz R and Gov N S 2008 *Biophys. J.* **94** 1155–68
- [63] Bobrovska N, Gózdź W, Kralj-Iglič V and Iglič A 2013 *PLoS ONE* **8** e73941
- [64] Spokoini R, Moldavski O, Nahmias Y, England J L, Schuldiner M and Kaganovich D 2012 *Cell Rep* **2** 738–47
- [65] Luby-Phelps K 1999 *International Review of Cytology* **192** 189–221
- [66] Binder B, Goede A, Berndt N and Holzhütter H G 2009 *PLoS ONE* **4** e8295
- [67] Hwang Y, Kumar P and Barakat A I 2014 *J. Math. Biol.* **69** 213–42
- [68] Hilioti Z, Sabbagh W, Paliwal S, Bergmann A, Goncalves M D, Bardwell L and Levchenko A 2008 *Curr. Biol.* **18** 1700–6
- [69] Baltanás R, Bush A, Couto A, Durrieu L, Hohmann S and Colman-Lerner A 2013 *Sci Signal* **6** ra26
- [70] Dohlman H G, Song J, Ma D, Courchesne W E and Thorner J 1996 *Mol. Cell. Biol.* **16**(9) 5194–209
- [71] Smith C, Pomiankowski A and Greig D 2014 *Behav. Ecol.* **25** 320–7
- [72] Lavi Y, Gov N, Edidin M and Gheber L A 2012 *Biophys. J.* **102** 1543–50
- [73] Hawkins R J, Bénichou O, Piel M and Voituriez R 2009 *Phys Rev E Stat Nonlin Soft Matter Phys.* **80** 040903
- [74] Elliott C M, Stinner B and Venkataraman C 2012 *J R Soc Interface* **9** 3027–44
- [75] Ku C J, Wang Y, Pavie B, Altschuler S J and Wu L F 2010 On identifying information from image-based spatial polarity phenotypes in neutrophils *ISBI (IEEE)* **1029** 32
- [76] Bastian P, Blatt M, Dedner A, Engwer C, Klöfkorner R, Kornhuber R, Ohlberger M and Sander O 2008 *Computing* **82** 121–38 ISSN 0010-485X
- [77] Geuzaine C and Remacle J F 2009 *International Journal for Numerical Methods in Engineering* **79** 1309–1331